

Analysis of Dirac Point in the Organic Conductor α -(BEDT-TTF) $_2$ I $_3$

Yoshikazu Suzumura

Department of Physics, Nagoya University, Chikusa-ku, Nagoya 464-8602, Japan

(Received March , 2016)

The Dirac electron in the organic conductor α -(BEDT-TTF) $_2$ I $_3$ under pressure is analyzed using a tight-binding model with nearest-neighbor transfer energies and four molecules per unit cell. By noting that the Dirac point between the first and second energy bands emerges or merges followed by the level crossing at a time-reversal invariant momentum (TRIM), an effective Hamiltonian is derived on the basis of these two wave functions at the TRIM, which have different parities associated with an inversion symmetry around the inversion center. We demonstrate that the Dirac point is determined by an intersection of two kinds of lines originating from the Hamiltonian described by symmetric and antisymmetric functions around the TRIM. The present method quantitatively gives a reasonable location of the Dirac point of α -(BEDT-TTF) $_2$ I $_3$ in a wide pressure range.

It is well known that the organic conductor α -(BEDT-TTF) $_2$ I $_3$ exhibits the Dirac point on the Fermi energy under pressure.¹⁾ By utilizing the energy band with such a Dirac cone, several studies have been performed to explore the properties of the Dirac electron.²⁾ However, in contrast to graphene,^{3,4)} it is not straightforward to obtain the Dirac point on the Brillouin zone owing to the accidental degeneracy at the Dirac point.⁵⁾

The existence of such a Dirac point is verified using a product of the parity at the time-reversal invariant momentum (TRIM),⁶⁻⁹⁾ and the merging or emergence of a pair of Dirac points occurs at the TRIM followed by level crossing.⁸⁾ The node of the component of the wave function¹⁰⁾ connects the Dirac point with the TRIM resulting in the Berry phase.¹¹⁾ Although the correspondence between the Dirac point and the TRIM has been clarified in these works, it is not yet successful to determine the location of the Dirac point except for the numerical diagonalization or semi-analytical calculation.¹²⁾ Thus, further study of the role of the TRIM is needed to elucidate the mechanism of the formation of the Dirac point. In this present paper, a method of finding the Dirac point is demonstrated using an effective Hamiltonian based on the parity of the wave function at the TRIM.

Figure 1 shows the structure of α -(BEDT-TTF) $_2$ I $_3$ with four molecules A, A', B, and C in the unit cell (the dot-dashed square), which gives a tight-binding model with seven kinds of nearest-neighbor transfer energies shown by a bond, a_1, \dots, b_4 .¹³⁾ There is an inversion symmetry around the sites of B, C, and the middle of A and A'. The tight-binding model of Fig. 1 is written as

$$\hat{H}_0 = \sum_{l,l'} \sum_{\alpha,\beta} |l'\beta\rangle t_{\alpha,\beta;l,l'} \langle l\alpha|, \quad (1)$$

where $|l\alpha\rangle$ denotes a state vector on the molecular site, and $t_{\alpha,\beta;l,l'}$ is the transfer energy between nearest-neighbor molecular sites. The quantities α and β denote the sites A, A', B, and C, and l and l' are the position vectors of the cell forming a square lattice with N sites. By using the Fourier transform

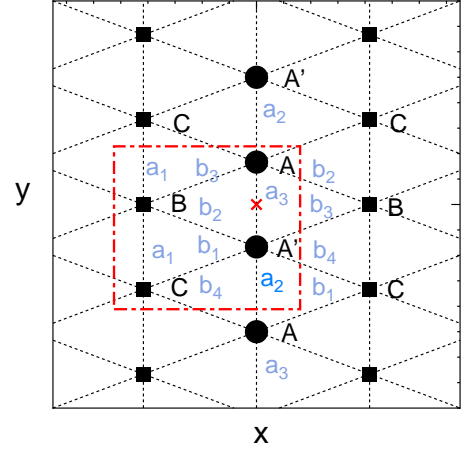


Fig. 1. (Color online) Structure of α -(BEDT-TTF) $_2$ I $_3$ on the x - y plane with four molecules A, A', B, and C per unit cell (dot-dashed square). The bond (dotted line) shows nearest-neighbor transfer energies, a_1, \dots, b_4 . The cross denotes an inversion center located at the middle of A and A' sites.¹³⁾

$|\mathbf{l}\alpha\rangle = N^{-1/2} \sum_{\mathbf{k}} \exp[i\mathbf{k}\mathbf{l}] |\mathbf{k}\alpha\rangle$ with a wave vector $\mathbf{k} = (k_x, k_y)$, Eq. (1) is rewritten as $\hat{H}_0 = \sum_{\mathbf{k}} |\Psi(\mathbf{k})\rangle H_S \langle \Psi(\mathbf{k})|$, where $|\Psi(\mathbf{k})\rangle = (2^{-1/2}(|\mathbf{k}A\rangle + |\mathbf{k}A'\rangle), 2^{-1/2}(|\mathbf{k}A\rangle - |\mathbf{k}A'\rangle), |\mathbf{k}B\rangle, |\mathbf{k}C\rangle)^t$ with H_S being a 4×4 matrix Hamiltonian.

By using a unitary transformation, $H_S(\mathbf{k})$ is rewritten as a real Hamiltonian,¹¹⁾

$$H(\mathbf{k}) = P(\mathbf{k})^{-1/2} H_S(\mathbf{k}) P(\mathbf{k})^{1/2} = \begin{pmatrix} \varepsilon_{11} & \varepsilon_{12} & \varepsilon_{13} & \varepsilon_{14} \\ \varepsilon_{21} & \varepsilon_{22} & \varepsilon_{23} & \varepsilon_{24} \\ \varepsilon_{31} & \varepsilon_{32} & \varepsilon_{33} & \varepsilon_{34} \\ \varepsilon_{41} & \varepsilon_{42} & \varepsilon_{43} & \varepsilon_{44} \end{pmatrix}, \quad (2)$$

where $\varepsilon_{11} = a_3 + a_2 \cos k_y$, $\varepsilon_{22} = -\varepsilon_{11}$, $\varepsilon_{12} = -a_2 \sin k_y$, $\varepsilon_{13} = \sqrt{2}(b_2 + b_3) \cos(k_x/2)$, $\varepsilon_{14} = \sqrt{2}b_1 \cos(\frac{k_x+k_y}{2}) + \sqrt{2}b_4 \cos(\frac{k_x-k_y}{2})$, $\varepsilon_{23} = \sqrt{2}(b_3 - b_2) \sin(k_x/2)$, $\varepsilon_{24} = -\sqrt{2}b_1 \sin(\frac{k_x+k_y}{2}) + \sqrt{2}b_4 \sin(\frac{k_x-k_y}{2})$, and $\varepsilon_{34} = 2a_1 \cos(k_y/2)$. $\varepsilon_{33} = \varepsilon_{44} = 0$ and $\varepsilon_{ij} = \varepsilon_{ji}$.

$P(\mathbf{k})$ denotes a matrix for the transformation of the base by a π -rotation around the inversion center, which is taken at the middle between A and A'. The elements of $P(\mathbf{k})$ are given by $[P(\mathbf{k})]_{\gamma,\gamma'} = p_\gamma(\mathbf{k})\delta_{\gamma,\gamma'}$ with $p_\gamma(\mathbf{k}) = 1, -1, e^{-ik_x}$, and $e^{-i(k_x+k_y)}$ for $\gamma = 1, 2, 3$, and 4, respectively. The equation for $P(\mathbf{k})$ is written as

$$P(\mathbf{k})|u_\gamma\rangle = p_\gamma(\mathbf{k})|u_\gamma\rangle, \quad (3)$$

which gives $p_\gamma(\mathbf{k}) = 1, -1, e^{-ik_x}, e^{-i(k_x+k_y)}$, and $|u_\gamma\rangle = (1, 0, 0, 0)^t, (0, 1, 0, 0)^t, (0, 0, 1, 0)^t, (0, 0, 0, 1)^t$, respectively. The TRIM is given by $\mathbf{k} = \mathbf{G}/2$ with \mathbf{G} being the reciprocal lattice vector, where $\mathbf{G}/2$ is written as $(k_x/\pi, k_y/\pi) = (0, 0)$ (Γ point), $(1, 0)$ (X point), $(0, 1)$ (Y point), and $(1, 1)$ (M point).

We mention two factors for deriving the effective Hamiltonian. One is the parity of the wave function at the TRIM, which is obtained by $P(\mathbf{G}/2)$.⁸⁾ Noting $p_\gamma(\mathbf{G}/2) = \pm 1$ in Eq. (3) and a relation

$$[P(\mathbf{G}/2), H(\mathbf{G}/2)] = 0, \quad (4)$$

one obtains

$$P(\mathbf{G}/2)|j(\mathbf{G}/2)\rangle = p_{E_j}(\mathbf{G}/2)|j(\mathbf{G}/2)\rangle, \quad (5)$$

$$H(\mathbf{G}/2)|j(\mathbf{G}/2)\rangle = E_j(\mathbf{G}/2)|j(\mathbf{G}/2)\rangle, \quad (6)$$

where $p_{E_j}(\mathbf{G}/2) = \pm 1$, and $E_1 > E_2 > E_3 > E_4$. Since the $+$ ($-$) sign gives the even (odd) parity for both $|u_\gamma\rangle$ and $|j(\mathbf{G}/2)\rangle$, the wave function $|j(\mathbf{G}/2)\rangle = \sum_\gamma d_{j\gamma}(\mathbf{G}/2)|u_\gamma\rangle$, with the even (odd) parity, is described by a linear combination of $|u_\gamma\rangle$ with even (odd) parity. The other is the relation between the parity and the matrix element of Eq. (2). When the parity of $|i(\mathbf{G}/2)\rangle$ is different from that of $|j(\mathbf{G}/2)\rangle$,

$$\begin{aligned} & \langle i(\mathbf{G}/2)|H(\mathbf{G}/2)|j(\mathbf{G}/2)\rangle \\ & = \sum_{\gamma_1, \gamma_2} d_{i\gamma_1}(\mathbf{G}/2)\varepsilon_{\gamma_1, \gamma_2} d_{j\gamma_2}(\mathbf{G}/2) = 0, \end{aligned} \quad (7)$$

leads to

$$\varepsilon_{\gamma_1, \gamma_2}(\mathbf{G}/2) = 0, \quad (8)$$

for $p_{\gamma_1}(\mathbf{G}/2)p_{\gamma_2}(\mathbf{G}/2) = -1$. In general, $\varepsilon_{\gamma_1, \gamma_2}(\mathbf{G}/2) \neq 0$ for $p_{\gamma_1}(\mathbf{G}/2)p_{\gamma_2}(\mathbf{G}/2) = 1$. Thus, for $p_{\gamma_1}(\mathbf{G}/2)p_{\gamma_2}(\mathbf{G}/2) = -1(+1)$, the matrix element $\varepsilon_{\gamma_1, \gamma_2}(\mathbf{k})$ with $\mathbf{k} = \mathbf{G}/2 + \mathbf{q}$ is antisymmetric (symmetric) as a function of \mathbf{q} owing to $E_j(\mathbf{G}/2 + \mathbf{q}) = E_j(\mathbf{G}/2 - \mathbf{q})$, i.e., the time-reversal symmetry. In the case of the Γ point ($\mathbf{G}/2=0$), the antisymmetric (symmetric) function with respect to \mathbf{k} is given by $\varepsilon_{12}(\mathbf{k}), \varepsilon_{23}(\mathbf{k})$, and $\varepsilon_{24}(\mathbf{k})$ (the others) in Eq. (2). When $|i(\mathbf{G}/2)\rangle$ and $|j(\mathbf{G}/2)\rangle$ have different parities, the quantity $\langle i(\mathbf{G}/2)|H(\mathbf{G}/2 + \mathbf{q})|j(\mathbf{G}/2)\rangle$ becomes antisymmetric as a function of \mathbf{q} , and then

$$\langle i(\mathbf{G}/2)|H(\mathbf{G}/2 + \mathbf{q})|j(\mathbf{G}/2)\rangle = 0, \quad (9)$$

gives a line passing through $\mathbf{G}/2$ owing to $\varepsilon_{\gamma_1, \gamma_2}$ being real.

Now, we examine the Dirac point between $E_1(\mathbf{k})$ and $E_2(\mathbf{k})$, which emerges at $\mathbf{k} = \mathbf{G}/2$ followed by a level crossing of $E_1(\mathbf{G}/2)$ and $E_2(\mathbf{G}/2)$ with different parities. Taking these $|1\rangle$ and $|2\rangle$ as the unperturbed

states where $E_j[\equiv E_j(\mathbf{G}/2)]$ and $|j\rangle [\equiv |j(\mathbf{G}/2)\rangle]$, we calculate $E_1(\mathbf{k})$ and $E_2(\mathbf{k})$ at an arbitrary \mathbf{k} by the perturbation of $V_{\mathbf{k}}$ defined as

$$V_{\mathbf{k}} = H_{\mathbf{k}} - H(\mathbf{G}/2), \quad (10)$$

and $H_{\mathbf{k}} = H(\mathbf{k})$. By extending our previous works,^{14, 15)} in which the base is taken at the Dirac point or the M point in the charge-ordered state, the effective Hamiltonian up to the second order is written as

$$H_{\text{eff}}(\mathbf{k}) = \begin{pmatrix} \langle 1|\tilde{H}_{\mathbf{k}}|1\rangle & \langle 1|\tilde{V}_{\mathbf{k}}|2\rangle \\ \langle 2|\tilde{V}_{\mathbf{k}}|1\rangle & \langle 2|\tilde{H}_{\mathbf{k}}|2\rangle \end{pmatrix}, \quad (11)$$

where $\tilde{H}_{\mathbf{k}} = H(\mathbf{G}/2) + \tilde{V}_{\mathbf{k}}$ and $\tilde{V}_{\mathbf{k}}$ is given by

$$\begin{aligned} \langle i|\tilde{V}_{\mathbf{k}}|j\rangle & = \langle i|V_{\mathbf{k}}|j\rangle + \frac{1}{2} \sum_{n=3,4} \langle i|V_{\mathbf{k}}|n\rangle \\ & \times \left(\frac{1}{E_i - E_n} + \frac{1}{E_j - E_n} \right) \langle n|V_{\mathbf{k}}|j\rangle. \end{aligned} \quad (12)$$

From Eq. (11), the energies $\tilde{E}_1(\mathbf{k})$ and $\tilde{E}_2(\mathbf{k})$ and the gap function $\Delta_{\mathbf{k}}$ are estimated as

$$\tilde{E}_j(\mathbf{k}) = \frac{\langle 1|\tilde{H}_{\mathbf{k}}|1\rangle + \langle 2|\tilde{H}_{\mathbf{k}}|2\rangle}{2} - (-1)^j \frac{\Delta_{\mathbf{k}}}{2}, \quad (13)$$

$$\Delta_{\mathbf{k}} = \tilde{E}_1(\mathbf{k}) - \tilde{E}_2(\mathbf{k}) = \sqrt{f(\mathbf{k})^2 + g(\mathbf{k})^2}, \quad (14)$$

where

$$f(\mathbf{k}) = 2 \langle 1|\tilde{H}_{\mathbf{k}}|2\rangle, \quad (15)$$

$$g(\mathbf{k}) = \langle 1|\tilde{H}_{\mathbf{k}}|1\rangle - \langle 2|\tilde{H}_{\mathbf{k}}|2\rangle. \quad (16)$$

The coupling between two bands of $\langle 1|\tilde{H}_{\mathbf{k}}|1\rangle$ and $\langle 2|\tilde{H}_{\mathbf{k}}|2\rangle$ vanishes on a line given by $f(\mathbf{k}) = 0$ [Eq. (9)], while $\langle 1|\tilde{H}_{\mathbf{k}}|1\rangle$ becomes equal to $\langle 2|\tilde{H}_{\mathbf{k}}|2\rangle$ on a line of $g(\mathbf{k}) = 0$, as will be shown later. The Dirac point $\pm\mathbf{k}_0$ is obtained from

$$\Delta_{\mathbf{k}_0} = 0, \quad (17)$$

which is equivalent to $f(\mathbf{k}_0) = 0$ and $g(\mathbf{k}_0) = 0$. The effective Hamiltonian [Eq. (11)] consisting of the anti-symmetric $f(\mathbf{k})$ and symmetric $g(\mathbf{k})$ has a common feature with that of $\text{Ca}_3\text{PbO}^{16)}$ in which the Dirac point is obtained using the $\text{Ca-}d_{x^2-y^2}$ and $\text{Pb-}p$ orbitals with different symmetries.

We numerically examine the case of α -(BEDT-TTF)₂I₃. The transfer energy $t = a_1, \dots, b_4$ (eV) at the uniaxial pressure P (kbar) is estimated as^{1, 17)}

$$t(P) = t(0)(1 + K_t P), \quad (18)$$

where $a_1(0), \dots, b_4(0) = -0.028, -0.048, 0.020, 0.123, 0.140, 0.062, 0.025$, and the corresponding K_t is given by $0.089, 0.167, -0.025, 0, 0.011$, and 0.032 , respectively.

The calculation of the Dirac point in terms of the states of the TRIMs ($\mathbf{G}/2 = \Gamma, X, Y$, and M) is performed as follows. (i) At a given pressure, verify the existence of the Dirac point using the condition $p_{E_1}(\Gamma)p_{E_1}(X)p_{E_1}(Y)p_{E_1}(M) = -1$.⁸⁾ (ii) Vary (increase

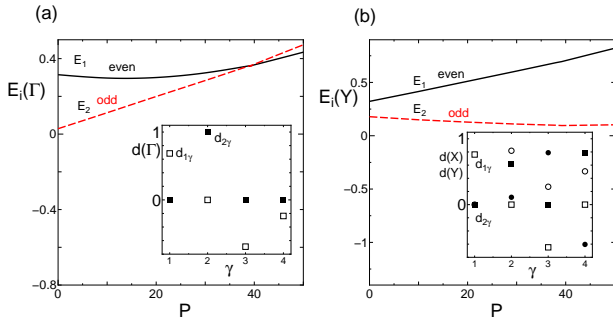


Fig. 2. (Color online) Pressure (P) dependence of $E_j(\mathbf{G}/2)$ ($j=1$ and 2) with the even or odd parity where $\mathbf{G}/2$ corresponds to the Γ point (a) and Y point (b). The inset shows components of $d_{j\gamma}(\mathbf{G}/2)$ for E_1 (open square) and E_2 (closed square) at $P=38$ kbar in (a), and at $P=4$ kbar in (b) where the open and closed circles in (b) denote $d_{j\gamma}(X)$ ($j=1$ and 2, respectively) at 4 kbar.

and decrease) pressure to obtain the TRIM at which the level crossing of $E_1(\mathbf{G}/2)$ and $E_2(\mathbf{G}/2)$ with different parities occurs. In this case, the Dirac point moves to the respective TRIM owing to the merging of a pair of Dirac points. (iii) Calculate the Dirac point by substituting the state of the TRIM into Eq. (17). One of these TRIMs is chosen depending on the location of the Dirac point.

The parity of the wave function in the present case is found as $[(p_{E1}(\mathbf{G}/2), p_{E2}(\mathbf{G}/2)] = (+, -), (-, -), (+, -)$, and $(+, -)$ at the Γ , X, Y, and M points respectively. Then the present method of Eq. (11) may be applied to the Γ , Y, and M points owing to $p_{E1}(\mathbf{G}/2)p_{E2}(\mathbf{G}/2) = -1$.

In Figs. 2(a) and 2(b), the pressure dependence of $E_j(\mathbf{G}/2)$ ($j=1$ and 2) is shown for the Γ and Y points where the level crossing of $E_1(\mathbf{k})$ and $E_2(\mathbf{k})$ occurs at the Γ point for $P = P_0$ ($= 39.2$ kbar), and at the Y point for $P = -11.8$ kbar (from the extrapolation), respectively. The Dirac point for $P \sim P_0$ is examined using the wave function of the Γ point, while the wave function of the Y point is applied to the Dirac point being far away from the Γ point. The inset denotes the corresponding $d_{j\gamma}(\Gamma)$ at $P = 38$ kbar (a) and $d_{j\gamma}(Y)$ at $P = 4$ kbar (b) [and $d_{j\gamma}(X)$ for comparison]. Each component has either the even parity or the odd parity. For the Γ point, the wave functions of E_1 , E_3 , and E_4 (E_2) have the even (odd) parity. For the Y point, the wave functions of E_1 and E_3 , (E_2 and E_4) have the even (odd) parity.

First, we show the merging behavior by taking Eq. (12) up to the first order for simplicity. Figure 3(a) shows $f(\mathbf{k})$ at $P=38$ kbar where $f(\mathbf{k}) = 0$ (the bright line) gives the merging direction, $k_y \simeq 0.07k_x$. Figure 3(b) shows the corresponding $g(\mathbf{k})$ where the bright line denotes $g(\mathbf{k}) = 0$, and $g(0) > 0$ at the Γ point. For $P > P_0$, the bright line moves from the horizontal axis to the vertical axis owing to $g(0) < 0$. Note that $g(\mathbf{G}/2) < 0$ for the X point and $g(\mathbf{G}/2) > 0$ for the Y and M points. The gap function $\Delta_{\mathbf{k}}$ [Eq. (14)] is obtained in Fig. 3(c) representing the contour just before the merging, which is slightly larger than that of the numerical diagonalization. The contour of $\Delta_{\mathbf{k}}$ close to the Dirac point is elliptic and the

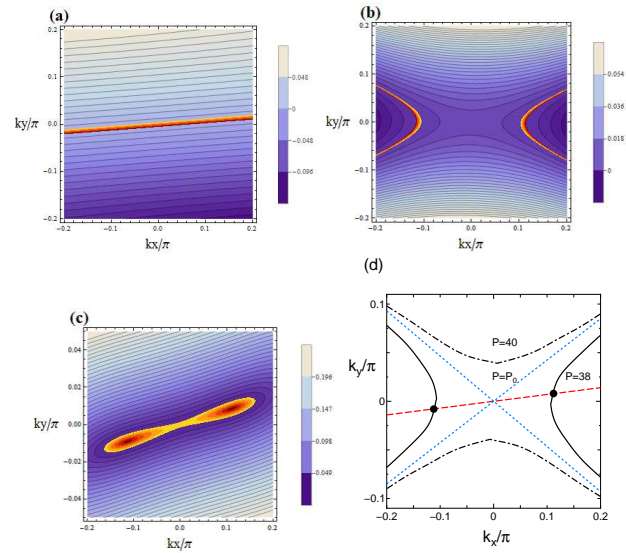


Fig. 3. (Color online) Contours of $f(\mathbf{k})$ (a) and $g(\mathbf{k})$ (b) at $P = 38$ kbar where the center $\mathbf{k} = 0$ denotes the Γ point. The bright line shows $f(\mathbf{k}) = 0$ and $g(\mathbf{k}) = 0$. With respect to the Γ point, $f(\mathbf{k})$ is antisymmetric and $g(\mathbf{k})$ is symmetric. The corresponding gap function of $\Delta_{\mathbf{k}}$ (c) shows a pair of Dirac points (in the bright region) just before the merging. In (d), the solid (dot-dashed) line denotes $g(\mathbf{k}) = 0$ at $P = 38$ kbar (40 kbar) and the dashed line denotes $f(\mathbf{k}) = 0$ for $P \simeq P_0$. The dotted line denotes $g(\mathbf{k}) = 0$ at $P = P_0$ ($= 39.2$ kbar).

principal axis is almost parallel to the merging direction. The merging at $\mathbf{G}/2$ is determined by $g(\mathbf{G}/2) = 0$, while $f(\mathbf{G}/2) = 0$ is the identity. Figure 3(d) shows the lines of $g(\mathbf{k}) = 0$ for $P = 38$ kbar (solid line) and 40 kbar (dot-dashed line), and $f(\mathbf{k}) = 0$ for $P \simeq P_0$ (dashed line). The dotted line denotes $g(\mathbf{k}) = 0$ at $P = P_0$, which is given by $k_y \simeq (-0.02 \pm 0.045)k_x$. The Dirac point exists only for $P < P_0$ owing to the presence of an intersection between $f(\mathbf{k}) = 0$ and $g(\mathbf{k}) = 0$, which is shown by the closed circle with $(k_x/\pi, k_y/\pi) \simeq \pm(0.112, 0.008)$. The absence of the intersection for $P_0 < P$ leads to the formation of the gap in $\Delta_{\mathbf{k}}$. Figure 3(d) is also understood by the following analysis with $\mathbf{G}/2 = 0$ (the Γ point). For the pressure close to $P = P_0$, Eqs. (15) and (16) are expanded with respect to $\mathbf{q} (= \mathbf{k} - \mathbf{G}/2)$ as

$$g(\mathbf{k}) = D(P) - C_{2x}q_x^2 + 2C_{2xy}q_xq_y + C_{2y}q_y^2, \quad (19)$$

and $f(\mathbf{k}) \simeq -C_{1x}q_x + C_{1y}q_y$, where $D(P) \simeq D_0(P_0 - P)$. Figure 3(d) is well described by the parameters estimated as $D_0 \simeq 0.0039$, $C_{2x} \simeq 0.386$, $C_{2xy} \simeq 0.040$, and $C_{2y} \simeq 1.95$, $C_{1x} \simeq 0.04$, and $C_{1y} \simeq 0.56$.

Next, we examine the Dirac point by applying Eq. (12) up to the second-order perturbation. With decreasing pressure, the difference in \mathbf{k}_0 between the first- and second-order perturbations increases, and the choice of the Γ point becomes invalid at low pressure, e.g., the obtained Dirac point at $P=10$ kbar exhibits a different behavior. Thus, the Dirac point for lower pressures is calculated by taking the Y point where the matrix element with the antisymmetric function of $\mathbf{q} [= \mathbf{k} - (0, \pi)]$ is given by ε_{12} , ε_{14} , ε_{32} , and ε_{34} . Figure 4(a) shows $f(\mathbf{q})$ for $P = 4$ kbar corresponding to the pressure of the Dirac

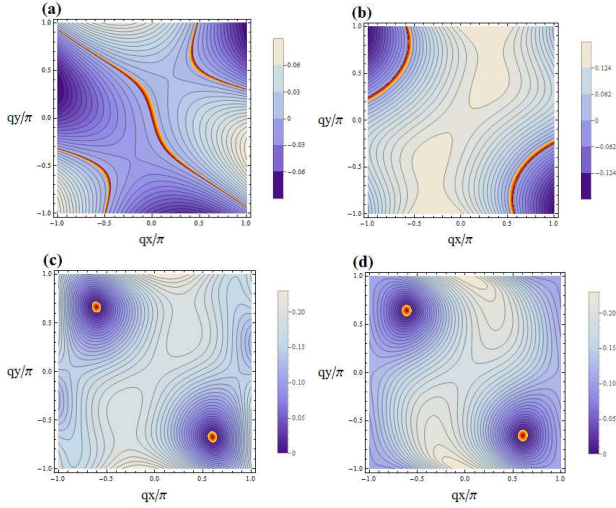


Fig. 4. (Color online) $\mathbf{q} [= \mathbf{k} - (0, \pi)]$ dependence of the contour for $f(\mathbf{q})$ (a), $g(\mathbf{q})$ (b), and $\Delta_{\mathbf{q}}$ (c) at $P=4$ kbar, which are obtained from Eqs. (15), (16), and (14) with $\mathbf{G}/2 = (0, \pi)$ (Y point). The center ($\mathbf{q} = 0$) denotes the Y point where $f(\mathbf{q})$ [$g(\mathbf{q})$] is antisymmetric (symmetric) with respect to \mathbf{q} . These (a) and (b) give $\Delta_{\mathbf{q}}$ in (c) and are compared with $\Delta_{\mathbf{q}}$ in (d), which is obtained from the numerical diagonalization of $H(\mathbf{k})$. The Dirac point in the bright region is given by $(q_x/\pi, q_y/\pi) = \pm(0.58, -0.67)$ for (c) and $\pm(0.60, -0.68)$ for (d).

electron found in α -(BEDT-TTF) $_2$ I $_3$.²⁾ The bright line obtained from $f(\mathbf{q}) = 0$ exists also for the second-order perturbation since the intermediate state $|n\rangle$ with $n = 3$ and 4 in Eq. (12) is orthogonal to either $|i\rangle$ or $|j\rangle$ with a different parity. Note that such a line exists in the presence and absence of the Dirac point, suggesting an intrinsic property that originates from the states $|i\rangle$ and $|j\rangle$ with a different parity. Figure 4(b) shows the corresponding $g(\mathbf{q})$ where $g(\mathbf{q}) = 0$ (the bright line) intersects with $f(\mathbf{q}) = 0$ in Fig. 4(a). The existence of the line of $g(\mathbf{q}) = 0$ is understood as follows. At the Y point (center), $g(\mathbf{q}) > 0$ from the definition, and $g(\mathbf{q}) < 0$ at the X point since $\langle 1|\tilde{H}_{\mathbf{k}}|1\rangle$ becomes smaller than $\langle 2|\tilde{H}_{\mathbf{k}}|2\rangle$ at the X point, as seen from the comparison of each component of the Y and X points in the inset of Fig. 2(b). Figure 4(c) shows $\Delta_{\mathbf{q}}$ [Eq. (14)], which is calculated from Figs. 4(a) and 4(b). Figure 4(d) shows $E_1(\mathbf{q}) - E_2(\mathbf{q})$, which is numerically calculated by the diagonalization of Eq. (2). The behavior around the Dirac point shows a good correspondence between Figs. 4(c) and 4(d), suggesting the validity of Eqs. (11) and (12) for finding the Dirac point.

Figure 5 shows the Dirac point on the plane of k_x and k_y with some choices of P (kbar). The closed circle is calculated by the numerical diagonalization of Eq. (2), where the Dirac point moves from the Γ point ($P = P_0$) to the Y point ($P = -11.8$ kbar) with decreasing pressure. The open square is obtained from Eq. (12) with the unperturbed state at the Γ point. Close to the Γ point, the difference between the closed circle and the open square is small, but increases with decreasing P . The open circle is obtained from Eq. (12) with the unperturbed state at the Y point. The difference between the closed circle

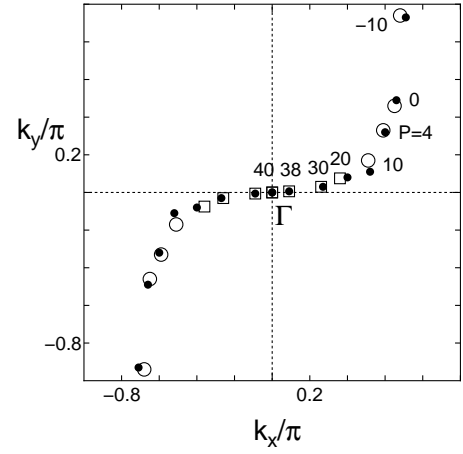


Fig. 5. Dirac point on the plane of k_x and k_y with some choices of P (kbar). The closed circle is the exact one and the open square (open circle) is obtained using the unperturbed state of the Γ point (Y point) in Eq. (12).

and the open circle is small but increases with increasing P from 10 kbar. As shown in Figs. 4(c) and 4(d), the Dirac point and the gap function $\Delta_{\mathbf{q}}$ at $P = 4$ kbar are well described by Eq. (11). Thus, the Dirac point is attributable to two ingredients given by Figs. 4(a) and 4(b), which exhibit the antisymmetric and symmetric functions with respect to the TRIM (of the Y point) and the resultant lines of $f(\mathbf{q}) = 0$ and $g(\mathbf{q}) = 0$. Finally, we note a range for using Eq. (13) where the region with $0 > \tilde{E}_1(\mathbf{k}) - E_1(\mathbf{k}) > -0.02$ covers a wide range including the Y and Γ points, and the Dirac point. However, although the location of the Dirac point is successfully obtained, the present method gives the overtilted Dirac cone for Fig. 4(c) owing to the first term of Eq. (13), and remains to be explored as the next step.

In summary, using an effective Hamiltonian based on two states with even and odd parities at the TRIM, we obtained the Dirac point as the intersection of two lines. One comes from the diagonal element with the symmetric function relevant to the crossing of two energy bands, and the other originates from the off-diagonal element with the antisymmetric function leading to the vanishing of the gap.

Acknowledgements

The author thanks R. Kato for useful discussions. This work was supported by a Grant-in-Aid for Scientific Research (A) (No. 15H02108) and (C) (No. 26400355) from the Ministry of Education, Culture, Sports, Science, and Technology, Japan,

- 1) S. Katayama, A. Kobayashi, and Y. Suzumura, J. Phys. Soc. Jpn. **75**, 054705 (2006).
- 2) K. Kajita, Y. Nishio, N. Tajima, Y. Suzumura, and A. Kobayashi, J. Phys. Soc. Jpn. **83**, 072002 (2014).
- 3) K. S. Novoselov, A. K. Geim, S. V. Morozov, D. Jiang, M. I. Katsnelson, I. V. Grigorieva, S. V. Dubonos, and A. A. Firsov, Nature **438**, 197 (2005).
- 4) For example, see the review by T. Ando, J. Phys. Soc. Jpn **74**, 777 (2005).

- 5) C. Herring, Phys. Rev. **52**, 365 (1937).
- 6) L. Fu and C. L. Kane, Phys. Rev. B **76**, 045302 (2007).
- 7) T. Mori, J. Phys. Soc. Jpn. **82**, 034712 (2013).
- 8) F. Piéchon and Y. Suzumura, J. Phys. Soc. Jpn. **82**, 033703 (2013).
- 9) T. Kariyado and Y. Hatsugai, Phys. Rev. B **88**, 245126 (2013).
- 10) A. Kobayashi and Y. Suzumura, J. Phys. Soc. Jpn. **82**, 054715 (2013).
- 11) F. Piéchon and Y. Suzumura, J. Phys. Soc. Jpn. **82**, 123703 (2013).
- 12) Y. Suzumura, T. Morinari, and F. Piéchon, J. Phys. Soc. Jpn. **82**, 023708 (2013).
- 13) T. Mori, A. Kobayashi, T. Sasaki, H. Kobayashi, G. Saito, and H. Inokuchi, Chem. Lett. **13**, 957 (1984).
- 14) S. Katayama, A. Kobayashi, and Y. Suzumura, Eur. Phys. J. B. **67**, 139 (2009).
- 15) A. Kobayashi, Y. Suzumura, F. Piéchon, and G. Montambaux, Phys. Rev. B **84**, 075450 (2011).
- 16) T. Kariyado and M. Ogata, J. Phys. Soc. Jpn. **80**, 083704 (2011); T. Kariyado and M. Ogata, J. Phys. Soc. Jpn. **81**, 064701 (2012).
- 17) R. Kondo, S. Kagoshima, and J. Harada, Rev. Sci. Instrum. **76**, 093902 (2005).